ELSEVIER

Journal of Organometallic Chemistry 556 (1998) 55–66

Journal of Organometallic Chemistry

Ferrocenyl substituted carboranes: synthesis and characterisation

Carsten L. Beckering, Georgina M. Rosair, Andrew S. Weller *

Department of Chemistry, Heriot-Watt University, Edinburgh, EH14 4AS, UK

Received 15 August 1997

Abstract

The reaction between ethynyl ferrocene and decaborane affords the new ferrocenyl substituted carborane 1-{*Fc*}-1,2-*closo*-$C_2B_{10}H_{11}$ **1** [$Fc = (\eta^5\text{-}C_5H_4)Fe(\eta^5\text{-}C_5H_5)$]. Deboronation of **1** gives K[7-{*Fc*}-7,8-*nido*-$C_2B_9H_{11}$] 2, and subsequent metallation, using the {Ru(*p*-cym)} fragment, affords the novel ferrocenyl substituted ruthenacarborane 1-{*Fc*}-3-(*p*-cym)-3,1,2-*closo*-$RuC_2B_9H_{10}$ **3** (*p*-cym = 1-Me–C_4H_4-4-^{i}Pr). Reaction between bis(methylethynyl)ferrocene and decaborane affords the bis carborane substituted ferrocene 1,1′-{*Fc′*}-{2-Me-1,2-*closo*-$C_2B_{10}H_{10}\}_2$, **4** [$Fc' = (\eta^5\text{-}C_5H_4)Fe(\eta^5\text{-}C_5H_4)$]. Deboronation of **4** results in the formation $[HNMe_3]_2$[7,7′-{*Fc′*}-{7-Me-7,8-*nido*-$C_2B_9H_{10}\}_2$], **5**, isolated as a *syn* and *anti* diastereoisomeric pair. Metallation of 5 affords the trimetallic ruthenacarborane 1,1-{*Fc′*}-{2-Me-3-(*p*-cym)-3,1,2-*closo*-$RuC_2B_9H_9\}_2$ **3**, as a mixture of *syn* and *anti* diastereoisomers. All the new complexes have been fully characterised by multinuclear NMR and micro-analysis, and for compounds **1**, **3**, **4** and *anti*-**6** by a single crystal X-ray study.

Keywords: Ferrocenyl; Carborane; Metallocaboranes; Ruthenacarborane

1. Introduction

The chemistry of functionalised metallocenes, especially ferrocene, is receiving considerable current attention, due to the electronic and magnetic properties that such complexes display [1,2]. Allied with this, much of the recent chemistry of carboranes and metallacarboranes has been directed towards their physical and electronic properties [3–5]. Attendant to the successful application of such systems is the ability to rationally synthesise targeted metallacaboranes which may display specific molecular and electronic properties. For example, R.N. Grimes and co-workers have elegantly demonstrated that molecular arrays consisting of metallacarborane units may be systematically assembled, using units based upon six and seven vertex metallacarboranes and analogous systems ([5]b, [6]). Surprisingly, an investigation of simple ferrocenyl substituted systems based upon the ubiquitous carborane *closo*-C_2B_{10} has been restricted to a single early report of the synthesis of 1-{$(\eta^5\text{-}C_5H_4)Fe(\eta^5\text{-}C_5H_5)$}-1,2-*closo*-$C_2B_{10}H_{11}$ [7], although we note the report of a cobaltacenium C-substituted *nido*-C_2B_9 [8] cage and various ferrocenyl B-substituted carboranes [9,10]. A very recent report also describes the synthesis of a zwitterionic compound which contains a $\{Ru(PPh_3)_2H\}^+$ fragment bound to the phenyl substituent on [7-Ph-*nido*-7,9-$C_2B_9H_{11}$]- [11].

We report here a preliminary investigation into the synthesis and characterisation of mono- and bis-carborane substituted ferrocenes. Their deboronation and subsequent metallation afford novel heterobi- and trimetallic ferrocenyl substituted metallacarboranes, which represent a starting point for the investigation of the synthesis and properties of metallocene-substituted (metalla)carboranes based upon C_2B_{10}.

* Corresponding author. Present address: Department of Chemistry and Biochemistry, University of Notre Dame, Notre Dame, Indiana 46556, USA; e-mail: Andrew.S.Weller.3@nd.edu

0022-328X/98/$19.00
PII S0022-328X(97)00676-1

2. Experimental

2.1. General

All experiments were carried out under a dry, oxygen-free dinitrogen atmosphere, using Schlenk-line techniques, although all the new compounds reported here are stable to the ambient atmosphere as both solutions and solids. All solvents were dried over appropriate drying agents and distilled immediately prior to use. Light petroleum refers to the fraction that boils between 40 and 60°C. Chromatography columns (3 × 15 cm) were packed with silica (Kieselgel 60, 200–400 mesh). Preparative Thin Layer Chromatography (TLC) was performed using glass plates coated with Kieselgel 60 F_{254} (0.2 mm thick) pre-washed with eluent. The compounds 1-{(η^5-C_5H_4)Fe(η^5-C_5H_5)}-1,2-*closo*-$C_2B_{10}H_{11}$ (compound **1**) [7] (η^5-C_5H_5)Fe(η^5-$C_5H_4C{\equiv}CH$) [12], Fe(η^5-$C_5H_4C{\equiv}CMe)_2$ [12] and [$RuCl_2$(*p*-cym)]$_2$ [13] were prepared by published procedures.

2.2. Spectroscopy

Proton NMR spectra were recorded on a Brüker AC 200 or a Brüker DPX 400 spectrometer, while $^{11}B\{^1H\}$ spectra were recorded on a Brüker DPX 400 spectrometer. Proton chemical shifts are reported relative to residual protio solvent in the sample, while ^{11}B chemical shifts are reported relative to $BF_3.OEt_2$ at 128.4 MHz. All the new complexes showed *J*(HB) coupling constants of ca. 140–150 Hz in their ^{11}B-NMR spectra.

2.3. Electrochemistry

Electrochemical measurements were carried out using an Autolab PGSTAT 20, driven by GPES4.3 (Eco Chemie) software, in CH_2Cl_2 solutions containing 0.4 mol dm^{-3} NBu_4BF_4 as supporting electrolyte. Cyclic voltametric experiments involved the use of a double platinum working electrode and a silver-wire reference electrode; all potentials quoted in the text are referenced to an internal ferrocene-ferrocenium standard and were obtained at a scan rate of 100 mVs^{-1}.

2.3.1. 1-{*Fc*}-1,2-*closo*-$C_2B_{10}H_{11}$], **1**

NMR data for complex 1: ^1H-NMR ($CDCl_3$) δ/ppm: 4.30 (m, 2 H, C_5H_4), 4.18 (s, 5 H, C_5H_5), 4.15 (m, 2 H, C_5H_4), 3.66 (s br, 1H, C_{cage}-H). $^{11}B\{1H\}$ ($CDCl_3$) δ/ppm: 1.11 (1 B), −2.20 (1 B), −6.79 (4 B, 2 + 2 coincident signal), −8.55 (2 B), −9.81 (2 B).

2.3.2. K[7-{*Fc*}-7,8-*nido*-$C_2B_9H_{11}$], **2**

Compound **1** (0.24 g, 0.7 mmol) was dissolved in degassed EtOH (20 cm^3), KOH (0.10 g, 1.8 mmol) was added, and the reaction mixture heated to reflux for 2 days. CO_2 was bubbled through the cooled solution and the resulting precipitate of K_2CO_3 was filtered off to afford a clear yellow solution. Removal of the solvent in vacuo and washing with light petroleum afforded an orange powder of analytically pure K[1-{*Fc*}-7,8-*nido*-$C_2B_9H_{11}$] (0.24 g, 0.66 mmol, 94%). $C_{12}H_{20}B_9FeK$ requires %H 5.65 %C 40.4. Found %H 4.92 %C 39.4.

NMR data for complex **2**: ^1H-NMR ($CDCl_3$) δ/ppm: 4.30 (m, 1 H, C_5H_4), 4.22 (s, 5 H, C_5H_5), 3.83 (m, 3 H, C_5H_4), 2.29 (s br, 1H, C_{cage}–H), −2.44 (br, 1H, B–H_{endo}). $^{11}B\{1H\}$[1]($CDCl_3$) δ/ppm: −7.24 (1 B), −7.68 (1 B), −9.81 (1 B), −13.33 (1 B), −14.07 (1 B), −15.93 (1 B), −20.72 (1 B), −30.51 (1 B), −32.63 (1 B).

2.3.3. 1-{*Fc*}-3-(*p*-cym)-3,1,2-*closo*-$RuC_2B_9H_{10}$, **3**

Compound **2** (0.91 g, 0.25 mmol) dissolved in thf (5 cm^3), was added to a suspension of pre-washed NaH (3.0 equivalents) in thf (10 cm^3). The mixture was heated to reflux for 3 h and the excess NaH allowed to settle. The resulting clear orange supernatent was decanted via syringe and added to a thf (10cm^3) solution of [$RuCl_2$(*p*-cym)]$_2$ (0.078 g, 0.12 mmol) and the solution stirred overnight. Solvent was removed in vacuo and the residue purified by thin layer chromatography (CH_2Cl_2:light petroleum 1:1) to afford a yellow band (*Rf* 0.85) of 1-{*Fc*}-3-(*p*-cym)-3,1,2-*closo*-$RuC_2B_9H_{10}$ (0.042 mg, 33%). $C_{21}H_{33}B_9FeRu$ requires %H 6.16 %C 46.7. Found %H 5.93 %C 46.6.

NMR data for Complex **3**: ^1H-NMR ($CDCl_3$) δ/ppm: 5.44 (m, 1 H, C_6H_4), 5.32 (m, 1 H, C_6H_4), 5.13 (m, 1 H, C_6H_4), 5.07 (m, 1 H, C_6H_4), 4.17 (m, 1 H, C_5H_4), 4.12 (s, 5H, C_5H_5), 4.20 (s br, 1 H, C_{cage}–H), 4.09 (m, 2 H, C_5H_4), 3.88 (m, 1 H, C_5H_4), 2.75 [qq, apparent heptet, 1 H, *p*-cym-CH, *J*(HH) 6,6 Hz], 2.21 (s, 3 H, Me-4), 1.23 [d, 3H, CH_3, *J*(HH) 6 Hz], 1.20 [d, 3 H, CH_3, *J*(HH) 6 Hz]; $^{11}B\{^1H\}$ ($CDCl_3$) δ/ppm: 4.74 (2 B, coincident), −0.61 (1 B), −4.75 (1 B), −6.53 (2 B, coincident), −11.59 (1 B), −15.40 (sh, 1 B), −16.48 (1 B).

2.3.4. 1,1′-{*Fc′*}-(2-*Me*-1,2-*closo*-$C_2B_{10}H_{10})_2$, **4**

Decaborane (0.63 g, 5.16 mmol) and *N*,*N*-dimethylaniline (0.76 g, 8.32 mmol) were stirred at room temperature (r.t.) in toluene (40 cm^3) for 1 h. Bis(methylethynyl)ferrocene (0.52 g, 2.10 mmol) was added and the solution heated to reflux for 3 h, over which time the solution turned black. The solvent was removed in vacuo and the residue taken up in CH_2Cl_2 (20 cm^3) and filtered through a silica plug. Removal of solvent and washing of the resulting orange precipitate with ice-cold methanol afforded 1,1′-{*Fc′*}-(2-Me-1,2-

[1] Peak at δ −30.51 ppm shows additional coupling in the ^{11}B-NMR spectrum (*ca.* 50 Hz) to the *endo* H atom associated with the open C_2B_3 face.

closo-$C_2B_{10}H_{10})_2$ (0.49 g, 50%). $C_{16}H_{34}B_{20}Fe$ requires %H 6.87 %C 38.6. Found %H 6.43 %C 37.9.

NMR data for Complex **4**: ^{1}H-NMR ($CDCl_3$) δ/ppm: 4.43 (m, 4 H, C_5H_4), 4.38 (m, 4 H, C_5H_4), 1.45 (s, 6 H, Me); $^{11}B\{^1H\}$ ($CDCl_3$) δ/ppm: 1.80 (2 B), 0.32 (2 B), −4.35 (12 B), −6.27 (4 B).

2.3.5. $[HNMe_3]_2[7,7'$-{*Fc'*}-(8-Me-7,8-*nido*-$C_2B_9H_{10})_2]$, **5**

Compound **4** (0.400 g, 0.803 mmol) was dissolved in degassed EtOH (20 cm^3), KOH (0.217, 4.02 mmol) was added, and the reaction mixture heated to reflux for 7 days. CO_2 was bubbled through the cooled solution and the resulting precipitate of K_2CO_3 was filtered off to afford a clear yellow solution. The ethanol was removed in vacuo, and the residue dissolved in H_2O (40 cm^3) and an aqueous solution of $[HNMe_3]Cl$ (0.38 g, 4.00 mmol) added, which resulted in the formation of a red/brown sticky precipitate. The solution was extracted three times with CH_2Cl_2 (3×30 cm^3), and the combined extracts dried over $MgSO_4$ to afford (0.397 g, 72%) of $[HNMe_3]_2[7,7'$-{*Fc'*}-(8-Me-7,8-*nido*-$C_2B_9H_{10})_2]$. $C_{22}H_{54}B_{18}FeN_2$ requires %H 9.12 %C 44.3. Found %H 8.65 %C 45.1.

NMR data for Complex **5**: ^{1}H-NMR ($CDCl_3$) δ/ppm: 4.10 − 3.71 (multiplets, 8 H, C_5H_4), 2.72 (s, 18 H, $HNMe_3$), 0.78 (s, Me), 0.72 (s, Me), −2.39 (br, 2 H, B–H_{endo}); $^{11}B\{^1H\}$ ($CDCl_3$) δ/ppm: −6.61 (4 B), −8.65 (2 B), −12.14 (2 B), −14.81 (2 B), −16.73 (2 B), −17.79 (2 B), −31.93 (2 B), −33.90 (2 B).

2.3.6. *1,1'*-{*Fc'*}-{2-Me-3-(*p*-cym)-3,1,2-*closo*-$RuC_2B_9H_9\}_2$, **6**

Compound **5** (0.200 g, 0.291 mmol) was deprotonated by overnight reflux with NaH (0.100 g, excess) in thf (40 cm^3). Excess NaH was left to settle and the clear orange supernatent decanted via syringe and added to an ice cooled thf solution (10 cm^3) of $[RuCl_2(p\text{-cym})]_2$ (0.178 g, 0.291 mmol). The solution was allowed to warm to r.t. and stirred for a total of 3 h. Solvent was removed in vacuo and the residue taken up in CH_2Cl_2 and filtered through a celite plug. The filtrate was evaporated to minimum volume and applied to a TLC plate. Elution with CH_2Cl_2/light petroleum (1:1) afforded an orange band of 1,1'-{*Fc'*}-{2-Me-3-(*p*-cym)-3,1,2-*closo*-$RuC_2B_9H_9\}_2$ (mass 0.030 g, 11%). Recrystallisation from CH_2Cl_2/light petroleum at 4°C afforded orange crystals of *anti*-1,1'-{*Fc'*}-{2-Me-3-(*p*-cym)-3,1,2-*closo*-$RuC_2B_9H_9\}_2$. $C_{36}H_{60}B_{18}FeRu_2$ requires %H 6.40 %C 43.7. Found %H 6.36 %C 43.4

NMR data for Complex **6**: <u>*Anti isomer*</u>- ^{1}H-NMR ($CDCl_3$) δ/ppm: 5.63 (m, 2 H, C_6H_4), 5.35 (m, 4 H, C_6H_4), 5.28 (m, 2 H, C_6H_4), 4.40 (m, 2 H, C_5H_4), 5.31 (m, 6 H, C_5H_4), 2.73 [qq, apparent heptet, 2 H, *p*-cym-CH, *J*(HH) 6,6 Hz], 2.52 (s, 6 H, Me), 2.13 (s, 6 H, Me), 1.29 [d, 6 H, Me, *J*(HH) 6], 1.24 [d, 6 H, Me, *J*(HH) 6]. $^{11}B\{^1H\}$ ($CDCl_3$) δ/ppm: 5.42 (6 B), −0.09 (4 B), −4.39 (2 B), −7.94 (2 B), −10.57 (4 B); <u>*Syn isomer*</u>- ^{1}H-NMR ($CDCl_3$) δ/ppm: 5.63 (m, 2 H, C_6H_4), 5.49 (m, 2 H, C_6H_4), 5.22 (m, 4 H, C_6H_4), 4.32 (m, 6 H, C_5H_4), 4.25 (m, 2 H. C_5H_4), 2.90 [qq, apparent heptet, 2 H, *p*-cym-CH, *J*(HH) 6,6 Hz], 2.48 (s, 6 H, Me), 2.12 (s, 6 H, Me), 1.29 [d, 6 H, Me, *J*(HH) 6], 1.24 [d, 6 H, Me, *J*(HH) 6].

2.4. Crystallography

Measurements on **1**, **3**, **4** and *anti*-**6** were carried out at r.t. on a Siemens P4 Diffractometer with graphite-monochromated Mo–K_α radiation ($\lambda = 0.71069$ Å) using ω scans. Structure solution and refinement were performed using the SHELXTL system [14] on a Pentium 90 MHz PC.

Table 1 lists details of unit cell data, intensity data collection and structure refinement. The unit cell parameters and orientation matrix for data collection for **1**, **3**, **4** and *anti*-**6** were determined by a least-squares refinement of 27, 23, 40 and 14 centred reflections, respectively, with 2θ ranging from 9.13 to 24.9°. Standard reflections were re-measured every 100 data and no significant crystal decay was found. Due to small crystal size, data for *anti*-**6** were collected only to $2\theta = 40°$. Data were corrected for absorption by psi scans. All structures were solved by direct and difference Fourier methods and refined by full-matrix least squares against F^2.

All phenyl, methyl and cyclopentadienyl hydrogen atom positions were calculated and treated as riding models. Terminal cage B–H atom positions were calculated and treated as riding models but the cage C-bonded H atoms were found in the difference map and the C–H distance was restrained to 1.15 Å. Phenyl, cyclopentadienyl and methyl H atom displacement parameters were treated as riding models with U_{iso} 1.2, 1.2 and 1.5 times the bound carbon atom $U_{eq.}$ respectively. Hydrogen atoms riding on all cage atoms were assigned displacement parameters 1.2 times the bound boron $U_{eq.}$ Data were weighted such that:

$$w^{-1} = [\sigma_c^2(F_o)^2 + (aP)^2 + [bP]$$

where

$$P = [0.333\max\{F_o^2, 0\} + 0.667F_c^2]$$

Tables 2, 4, 6 and 8 list fractional coordinates of non-H atoms for complexes **1**, **3**, **4** and *anti*-**6**, repectively, while selected bond lengths and angles are given in Tables 3, 5, 7 and 9 for the new complexes.

Atomic co-ordinates, thermal parameters, and bond lengths and angles have been deposited at the Cambridge Crystallographic Data Centre (CCDC). See Instructions for Authors, J. Organomet. Chem, 1998, Volume 555, Issue 1. Any request to the CCDC for this material should quote the full literature citation.

Table 1
Crystallographic fata for the new complexes **1**, **3**, **4** and **6**

	1	3	4	*anti*-6
Formula	$C_{12}H_{20}B_{10}Fe$	$C_{22}H_{33}B_9FeRu$	$C_{16}H_{34}B_{20}Fe$	$C_{36}H_{60}B_{18}FeRu_2$
M	328.23	551.69	498.48	945.41
System	Monoclinic	Triclinic	Monoclinic	Monoclinic
Space group	$P2_1/c$	$P-1$	$P2_1/n$	$P2_1/c$
Unit cell dimensions				
a (Å)	19.4270(10)	9.194(2)	7.5054(10)	12.982(4)
b (Å)	13.3990(10)	11.649(3)	22.203(2)	11.495(5)
c (Å)	12.8750(10)	12.482(3)	7.9545(9)	15.056(3)
α (°)	90	111.61(2)	90	90
β (°)	95.660(10)	92.84(2)	96.821(10)	110.09(3)
γ (°)	90	91.23(2)	90	90
V (Å^3)	3335.1(4)	1240.2(5)	1316.2(2)	2110.1(12)
Temperature (K)	293(2)	293(2)	293(2)	293(2)
Z	8	2	2	2
Crystal dimensions (mm)	$0.3\times0.3\times0.4$	$0.2\times0.2\times0.3$	$0.2\times0.3\times0.4$	$0.1\times0.2\times0.2$
$D_{calc.}$ (g cm^{-3})	1.307	1.477	1.258	1.488
μ(Mo–K$_\alpha$) (mm^{-1})	0.889	1.204	0.582	1.075
F(000) (e)	1344	560	512	960
2θ range (°)	3–50	3–50	3–50	2–40
No. of unique data collected	5183	4216	2300	2739
No. data used in refinement	5181	4216	2300	2739
wR_2 ($RI>2\sigma(I)$)	0.1049 (0.0519)	0.1286 (0.0549)	0.1171 (0.0476)	0.1500 (0.0698)
S	1.029	1.056	1.077	1.066
a	0.0492	0.0631	0.0659	0.0895
b	0.46	0	0	0.37
Max residue (e Å^{-3})	+0.289	+1.037	+0.408	+1.116
Min residue (e Å^{-3})	−0.266	−0.700	−0.338	−0.576

$R=\Sigma||F_o|-|F_c||/\Sigma|F_o|$.
$Rw_2=\{\Sigma[w(F_o^2-F_c^2)^2]/\Sigma[w(F_o^2)^2]\}^{1/2}$, $w=\sigma^2(F_o^2)+(aP)^2+bP$, $P=[F_o^2+2F_c^2]/3$.
$S=[\Sigma[w(F_o^2-F_c^2)^2]/(n-p)]^{1/2}$ where n = no. data and p = no. variables.

3. Results and discussion

3.1. Synthesis and characterisation of monosubstituted carboryl ferrocenes

An early report by Zakharkin et al. describes the synthesis of 1-{(η^5-C_5H_4)Fe(η^5-C_5H_5)}-1,2-*closo*-$C_2B_{10}H_{11}$ [7] Scheme 1, by heating to reflux a toluene solution of $B_{10}H_{14}$ and ethynyl ferrocne in the presence of acetonitrile catalyst. However, full spectroscopic characterisation and the solid-state structure were not reported, and for comparison with the new complexes reported here, we have synthesised 1-{*Fc*}-1,2-*closo*-$C_2B_{10}H_{11}$ (compound **1**) and fully characterised it by ^{1}H-, ^{11}B{^{1}H}-NMR spectroscopy and single crystal X-ray diffraction.

In the ^{1}H-NMR spectrum two, integral two, multiplets are observed for the (η^5-C_5H_4) group, as well as the expected integral five singlet for (η^5-C_5H_5) and a broad, integral one signal assigned to the cage CH proton. The ^{11}B{^{1}H}-NMR spectrum shows five resonances between 1.11 and −9.81 ppm in the ratio 1:1:4:2:2 (the integral four resonance due to a 2 + 2 coincidence), in the region associated with *closo*-C_2B_{10} icosahedra, demonstrating that the molecule has a mirror plane of symmetry in solution. Fig. 1 shows a perspective view of compound **1**, showing the numbering scheme adopted, while Table 3 gives selected bond lengths and angles.

Compound **1** crystallises as two crystallographically independent molecules in the unit cell [**1** and **1′**], with no close intramolecular contacts. The unsubstituted cage carbon atom, C(2) [C(2′) in molecule **1′**], was unambiguously identified from a combination of isotropic thermal parameters and bond lengths. The cage carbon bond length, C(1)–C(2) 1.672(7) Å [1.657(6) Å] is slightly longer than those found in [1-Ph-1,2-*closo*-$C_2B_{10}H_{11}$], [15] at 1.649(2) and 1.640(5) Å in two different crystalline modifications. Boron–boron bond lengths range between 1.724(10)–1.779(10) Å [1.759(7)–1.789(8) Å], while carbon–boron lengths range between 1.687(7)–1.730(8) Å [1.695(7)–1.721(7) Å]. The C(1)–C(11) bond length at 1.487(7) Å [1.498(6) Å] is slightly longer than that found in the only other crystallographically characterised C-substituted metallocene/carborane complex 7-{(η^5-C_5H_4)Co(η^5-C_5H_5)}-7,8-*nido*-$C_2B_9H_{10}$ [8] at 1.4803(16) Å. The appended ferrocenyl group is orientated so that the molecule overall lacks a plane of mirror symmetry in the solid state, demonstrating that free rotation, or at least libra-

tion, around the C(1)–C(11) connectivity is occurring in solution to afford the observed C_s symmetry in the NMR spectra. The Fe–C distances range between 2.016(7) and 2.044(6) Å for Fe(1)–C(11) to C(15) [2.032(5)–2.049(5) Å] and between 2.010(7) and 2.031(7) Å for Fe(1)–C(21) to C(25) [2.019(5)–2.050(5) Å]. Carbon–carbon bond lengths in the upper cyclopentadienyl ring, C(11)–C(15), lie in the range 1.396(8)–1.431(6) Å [1.409(7)–1.428(6) Å], while those in the lower ring, C(21)–C(25), span a larger range between 1.315(12) and 1.459(13) Å [1.378(8)–1.421(9) Å], presumably due to the greater thermal libration associated with the lower cyclopentadienyl ring.

Table 2
Atomic coordinates ($\times 10^4$) and equivalent isotropic displacement parameters ($Å^2 \times 10^3$) for **1** and **1′**

	x	*y*	*z*	U_{eq}
Fe(1)	2671(1)	−689(1)	888(1)	54(1)
C(1)	3888(2)	819(4)	1809(3)	49(1)
C(2)	4531(3)	−7(4)	1787(5)	71(2)
B(3)	4168(3)	183(5)	2930(5)	64(2)
B(4)	3996(3)	1445(5)	2950(4)	59(2)
B(5)	4209(4)	2012(5)	1820(5)	61(2)
B(6)	4545(3)	1071(5)	1051(5)	61(2)
B(7)	5071(3)	32(5)	2922(6)	68(2)
B(8)	4730(4)	988(5)	3669(5)	68(2)
B(9)	4757(4)	2113(5)	2983(6)	69(2)
B(10)	5111(4)	1871(5)	1792(6)	73(2)
B(11)	5300(3)	592(6)	1758(6)	71(2)
B(12)	5440(4)	1233(5)	2947(6)	72(2)
C(11)	3176(2)	601(4)	1327(3)	48(1)
C(12)	2580(3)	481(4)	1863(4)	65(2)
C(13)	1998(3)	419(4)	1105(5)	74(2)
C(14)	2230(3)	502(4)	117(5)	70(2)
C(15)	2953(3)	621(4)	234(4)	62(1)
C(21)	2104(4)	−1955(6)	783(11)	114(3)
C(22)	2517(7)	−1974(6)	1655(8)	127(4)
C(23)	3175(6)	−1928(5)	1428(11)	117(4)
C(24)	3196(5)	−1877(5)	382(11)	123(4)
C(25)	2473(7)	−1874(6)	−53(7)	117(3)
Fe(1′)	2333(1)	4445(1)	1083(1)	44(1)
C(1′)	1001(2)	3687(3)	2222(3)	36(1)
C(2′)	635(3)	3096(4)	1179(4)	47(1)
B(3′)	353(3)	4261(4)	1433(4)	48(1)
B(4′)	398(3)	4328(4)	2822(4)	45(1)
B(5′)	732(3)	3189(4)	3329(4)	43(1)
B(6′)	910(3)	2413(4)	2274(4)	48(1)
B(7′)	−239(3)	3303(5)	1011(4)	59(2)
B(8′)	−406(3)	4072(5)	2072(5)	57(2)
B(9′)	−166(3)	3399(5)	3242(4)	53(1)
B(10′)	156(3)	2208(4)	2911(5)	53(1)
B(11′)	117(3)	2156(4)	1518(5)	56(2)
B(12′)	−545(3)	2761(5)	2128(5)	60(2)
C(11′)	1718(2)	4101(3)	2229(3)	40(1)
C(12′)	2350(2)	3554(4)	2378(3)	51(1)
C(13′)	2896(3)	4250(5)	2486(4)	61(1)
C(14′)	2618(3)	5217(5)	2415(4)	68(2)
C(15′)	1880(3)	5138(4)	2247(4)	54(1)
C(21′)	2094(3)	5209(5)	−281(4)	71(2)
C(22′)	1858(3)	4236(5)	−395(4)	66(2)
C(23′)	2433(4)	3601(5)	−205(4)	77(2)
C(24′)	3021(3)	4220(6)	30(4)	83(2)
C(25′)	2798(3)	5208(5)	−14(4)	74(2)

U_{eq} is defined as one third of the trace of the orthogonalized U_{ij} tensor.

Table 3
Selected bond lengths [Å] and angles [°] for **1** and **1′**

Fe(1)–C(11)	2.041(5)	Fe(1′)–C(11′)	2.041(4)
Fe(1)–C(12)	2.028(5)	Fe(1′)–C(12′)	2.049(5)
Fe(1)–C(13)	2.016(5)	Fe(1′)–C(13′)	2.034(5)
Fe(1)–C(14)	2.025(5)	Fe(1′)–C(14′)	2.032(5)
Fe(1)–C(15)	2.044(6)	Fe(1′)–C(15′)	2.034(5)
Fe(1)–C(21)	2.020(8)	Fe(1′)–C(21′)	2.047(6)
Fe(1)–C(22)	2.022(8)	Fe(1′)–C(22′)	2.050(5)
Fe(1)–C(23)	2.016(7)	Fe(1′)–C(23′)	2.033(5)
Fe(1)–C(24)	2.031(7)	Fe(1′)–C(24′)	2.019(5)
Fe(1)–C(25)	2.010(7)	Fe(1′)–C(25′)	2.028(5)
C(1)–C(11)	1.487(7)	C(1′)–C(11′)	1.498(6)
C(1)–C(2)	1.672(7)	C(1′)–C(2′)	1.657(6)
C(11)–C(12)	1.415(7)	C(11′)–C(12′)	1.428(6)
C(11)–C(15)	1.431(6)	C(11′)–C(15′)	1.425(6)
C(12)–C(13)	1.420(7)	C(12′)–C(13′)	1.409(7)
C(13)–C(14)	1.396(8)	C(13′)–C(14′)	1.404(8)
C(14)–C(15)	1.407(8)	C(14′)–C(15′)	1.431(7)
C(21)–C(25)	1.356(12)	C(21′)–C(25′)	1.378(8)
C(21)–C(22)	1.315(12)	C(21′)–C(22′)	1.384(8)
C(22)–C(23)	1.341(13)	C(22′)–C(23′)	1.406(9)
C(23)–C(24)	1.353(13)	C(23′)–C(24′)	1.421(9)
C(24)–C(25)	1.459(13)	C(24′)–C(25′)	1.392(9)
Cp1–Fe(1)[a]	1.636	Cp1′–Fe(1′)	1.649
Cp2–Fe(1)	1.687	Cp2′–Fe(1′)	1.653
C(12)–C(11)–C(15)	107.3(4)	C(15′)–C(11′)–C(12′)	108.2(4)
C(12)–C(11)–C(1)	126.3(4)	C(12′)–C(11′)–C(1′)	126.7(4)
C(15)–C(11)–C(1)	125.8(5)	C(15′)–C(11′)–C(1′)	124.4(4)
C(11)–C(12)–C(13)	107.9(5)	C(13′)–C(12′)–C(11′)	107.6(5)
C(14)–C(13)–C(12)	108.4(5)	C(14′)–C(13′)–C(12′)	108.9(5)
C(13)–C(14)–C(15)	108.6(5)	C(13′)–C(14′)–C(15′)	108.4(5)
C(14)–C(15)–C(11)	107.9(5)	C(11′)–C(15′)–C(14′)	107.0(5)
C(22)–C(21)–C(25)	110.7(9)	C(25′)–C(21′)–C(22′)	109.6(6)
C(21)–C(22)–C(23)	109.2(10)	C(21′)–C(22′)–C(23′)	107.7(6)
C(22)–C(23)–C(24)	110.0(10)	C(22′)–C(23′)–C(24′)	107.0(5)
C(23)–C(24)–C(25)	105.1(9)	C(25′)–C(24′)–C(23′)	107.8(6)
C(21)–C(25)–C(24)	105.0(8)	C(21′)–C(25′)–C(24′)	107.9(6)
C(11)–C(1)–C(2)	121.9(4)	C(11′)–C(1′)–C(2′)	120.5(3)
C(11)–C(1)–B(4)	119.4(4)	C(11′)–C(1′)–B(4′)	119.5(4)
C(11)–C(1)–B(6)	121.0(4)	C(11′)–C(1′)–B(5′)	120.1(4)
C(11)–C(1)–B(5)	120.6(4)	C(11′)–C(1′)–B(6′)	117.8(4)
C(11)–C(1)–B(3)	117.2(4)	C(11′)–C(1′)–B(3′)	117.7(3)
Cp(1)–Fe(1)–Cp(2)	170.4	Cp(1′)–Fe(1′)–Cp(2′)	174.8

[a] Cp1 and Cp2 refer to the computed ring centriods for the cyclopentadienyl rings C(11)–C(15) and C(21)–C(25), respectively.

Previously in systems based upon aryl substituted carboranes, the twist of the aryl group has been described by the parameter θ [16]. In compound **1**, the ferrocenyl group is twisted by $\theta = 18.2°$, where $\theta = 90°$ is equivalent to the upper cyclopentadienyl ring lying essentially co-planar with the cage carbon atoms. This is significantly different from that found in 1-Ph-1,2-*closo*-$C_2B_{10}H_{11}$ [15] where $\theta = 67°$. It is interesting to note that the conformation adopted in both independent molecules, **1** and **1′**, is essentially the same, sug-

gesting that electronic factors are important in determining the orientation of the appended ferrocenyl group. Additionally one of the hydrogens on the lower cyclopentadienyl ring [C(21)–C(25)] fits between two of the hydrogen atoms on the carborane cage i.e. H(23B) on the lower cyclopentadienyl ring and H(2) and H(3) on the cage. For molecule **1**, H(23B)–H(3) is 2.738 Å, and H(23B)–H(2) is 2.572 Å. Overall, this perhaps suggests that the conformation adopted by the ferrocenyl group is a combination of steric and electronic factors, as found previously for analogous aryl substituted carborane systems ([15]a).

Deboronation of complex **1**, by standard procedures [17], afforded K[7-{*Fc*}-7,8-*nido*-7,8-$C_2B_9H_{11}$] **2**, in excellent yield. ^{1}H and ^{11}B{^{1}H}-NMR spectroscopy confirmed the formulation of this new complex. Thus, the ^{11}B{^{1}H}-NMR spectrum displays nine inequivalent boron environments between δ −7.24 and δ −32.63 ppm in the range associated with *nido*-C_2B_9 cages, while in the ^{1}H-NMR spectrum the η-C_5H_4 ring is now observed as two multiplets in the ratio 1:3, with a broad peak observed at δ −2.44 ppm due to the hydrogen atom associated with the open C_2B_3 face.

Complex **2** is a precursor for the construction of heterometallic complexes based upon ferrocenyl substituted *nido*-C_2B_9 cages. Deprotonation with NaH and subsequent reaction with [$RuCl_2$(*p*-cym)]$_2$ affords the novel ferrocenyl ruthenacarborane 1-{*Fc*}-3-(*p*-cym)-3,1,2-*closo*-$RuC_2B_9H_{10}$ **3** in moderate yield after preparative thin layer chromatography. Complex **3** was initially characterised by spectroscopic techniques. The ^{11}B{^{1}H}-NMR spectrum shows seven resonances (two coincident) between δ 4.74 and δ −16.48 ppm, indicative of a *closo*-MC_2B_9 cage architecture, while in the ^{1}H-NMR spectrum signals are observed due to *p*-cym and ferrocenyl groups that are fully consistent with the formulation of the molecule. Noteably, the *p*-cymene group is observed as four, integral one, multiplets between δ 5.44 and δ 5.07 ppm, an integral one quartet of quartets (virtual septet) at δ 2.75 ppm, an integral three singlet at δ 2.21 ppm and two, integral three, doublets

Table 4
Atomic coordinates ($\times 10^4$) and equivalent isotropic displacement parameters (Å$^2 \times 10^3$) for **3**

	x	*y*	*z*	U_{eq}
Fe(1)	7369(1)	12184(1)	8794(1)	38(1)
Ru(3)	6444(1)	7597(1)	6668(1)	24(1)
C(1)	5629(7)	9474(5)	7406(5)	25(1)
C(2)	5442(7)	8864(6)	5979(6)	29(1)
B(4)	4881(8)	8460(7)	7980(6)	27(1)
B(5)	3952(8)	9794(6)	7984(6)	30(1)
B(6)	4332(8)	10068(7)	6708(7)	32(2)
B(7)	4540(7)	7406(7)	5479(6)	28(2)
B(8)	4115(7)	7127(7)	6761(7)	31(2)
B(9)	2977(7)	8345(7)	7564(6)	30(1)
B(10)	2655(8)	9336(7)	6784(7)	35(2)
B(11)	3637(8)	8776(7)	5510(7)	32(2)
B(12)	2774(7)	7710(7)	6026(7)	32(2)
C(30)	7824(10)	7097(8)	9035(7)	51(2)
C(31)	7933(7)	6933(7)	7779(6)	37(2)
C(32)	7214(7)	5913(6)	6884(6)	36(2)
C(33)	7299(7)	5787(6)	5723(6)	34(2)
C(34)	8108(7)	6644(7)	5390(6)	37(2)
C(35)	8815(7)	7663(7)	6309(7)	35(2)
C(36)	8733(7)	7794(6)	7459(7)	38(2)
C(37)	8160(9)	6443(8)	4120(7)	49(2)
C(38)	9170(10)	5393(9)	3564(8)	58(2)
C(39)	8601(15)	7567(11)	3884(10)	81(3)
C(41)	6911(7)	10297(6)	8002(5)	27(1)
C(42)	8085(7)	10693(6)	7494(6)	35(1)
C(43)	9229(8)	11236(7)	8378(7)	43(2)
C(44)	8730(8)	11197(7)	9425(6)	43(2)
C(45)	7318(7)	10640(6)	9209(6)	33(1)
C(51)	5524(14)	13175(9)	8922(12)	79(3)
C(55)	6302(15)	13561(9)	9988(10)	78(3)
C(54)	7651(15)	14002(9)	9838(12)	85(4)
C(53)	7729(17)	13850(9)	8672(13)	93(4)
C(52)	6331(18)	13341(9)	8124(11)	87(4)

U_{eq} is defined as one third of the trace of the orthogonalized U_{ij} tensor.

Table 5
Selected bond lengths [Å] and angles [°] for **3**

Fe(1)–C(53)	2.023(9)	Fe(1)–C(44)	2.035(8)
Fe(1)–C(54)	2.039(10)	Fe(1)–C(43)	2.040(8)
Fe(1)–C(42)	2.041(7)	Fe(1)–C(45)	2.047(7)
Fe(1)–C(55)	2.051(10)	Fe(1)–C(51)	2.051(11)
Fe(1)–C(52)	2.057(11)	Fe(1)–C(41)	2.075(6)
Ru(3)–C(2)	2.163(6)	Ru(3)–C(33)	2.187(7)
Ru(3)–B(7)	2.190(7)	Ru(3)–B(4)	2.200(7)
Ru(3)–C(1)	2.201(6)	Ru(3)–C(32)	2.203(6)
Ru(3)–B(8)	2.218(7)	Ru(3)–C(31)	2.246(6)
Ru(3)–C(36)	2.250(6)	Ru(3)–C(35)	2.252(6)
Ru(3)–C(34)	2.264(7)	C(1)–C(41)	1.484(8)
C(31)–C(36)	1.414(10)	C(31)–C(32)	1.419(10)
C(32)–C(33)	1.408(10)	C(33)–C(34)	1.423(11)
C(34)–C(35)	1.428(10)	C(34)–C(37)	1.518(11)
C(35)–C(36)	1.392(11)	C(37)–C(39)	1.497(14)
C(37)–C(38)	1.525(11)	C(41)–C(42)	1.428(9)
C(41)–C(45)	1.438(9)	C(42)–C(43)	1.438(10)
C(43)–C(44)	1.423(11)	C(44)–C(45)	1.406(10)
C(51)–C(52)	1.34(2)	C(51)–C(55)	1.39(2)
C(55)–C(54)	1.38(2)	C(54)–C(53)	1.41(2)
C(53)–C(52)	1.43(2)		
Cp1–Fe(1)	1.649	Cp2–Fe(1)	1.668
C(41)–C(1)–C(2)	120.7(5)	C(42)–C(41)–C(45)	107.3(5)
C(41)–C(1)–B(4)	120.6(5)	C(41)–C(42)–C(43)	108.1(6)
C(41)–C(1)–B(6)	116.9(5)	C(44)–C(43)–C(42)	107.3(6)
C(41)–C(1)–B(5)	119.1(5)	C(45)–C(44)–C(43)	109.0(6)
C(41)–C(1)–Ru(3)	106.2(4)	C(44)–C(45)–C(41)	108.2(6)
C(2)–Ru(3)–B(4)	79.0(3)	C(52)–C(51)–C(55)	110.8(12)
C(2)–Ru(3)–C(1)	44.6(2)	C(54)–C(55)–C(51)	106.8(12)
B(4)–Ru(3)–C(1)	46.5(2)	C(55)–C(54)–C(53)	108.9(12)
C(2)–Ru(3)–B(8)	80.4(3)	C(54)–C(53)–C(52)	105.9(11)
B(4)–Ru(3)–B(8)	48.8(3)	C(51)–C(52)–C(53)	107.6(11)
C(2)–Ru(3)–B(7)	47.5(2)	C(1)–Ru(3)–B(8)	80.6(3)
B(7)–Ru(3)–B(4)	82.7(3)	B(7)–Ru(3)–C(1)	80.1(3)
Cp1–Fe(1)–Cp(2)	178.7	B(7)–Ru(3)–B(8)	48.3(3)

Table 6
Atomic coordinates ($\times 10^4$) and equivalent isotropic displacement parameters ($Å^2 \times 10^3$) for **4**

	x	y	z	U_{eq}
Fe(1)	5000	5000	10 000	32(1)
C(1)	2306(5)	6032(2)	8242(4)	27(1)
C(2)	1129(5)	6669(2)	8638(5)	32(1)
B(3)	2924(6)	6729(2)	7495(6)	36(1)
B(4)	2899(6)	6068(2)	6232(5)	35(1)
B(5)	1090(6)	5608(2)	6730(5)	34(1)
B(6)	29(6)	5988(2)	8301(6)	35(1)
B(7)	892(7)	7128(2)	6912(6)	42(1)
B(8)	1984(7)	6754(2)	5362(6)	42(1)
B(9)	827(7)	6063(2)	4878(6)	42(1)
B(10)	−944(7)	6007(2)	6168(7)	42(1)
B(11)	−896(6)	6672(2)	7420(6)	41(1)
B(12)	−400(7)	6715(2)	5292(6)	45(1)
C(11)	3505(5)	5786(2)	9703(4)	31(1)
C(12)	5387(6)	5925(2)	10 077(6)	43(1)
C(13)	6004(7)	5668(2)	11 650(6)	55(1)
C(14)	4576(8)	5373(2)	12 269(5)	57(1)
C(15)	3016(7)	5437(2)	11 072(5)	43(1)
C(20)	1334(7)	6912(2)	10 429(5)	44(1)

Symmety transformations used to generate equivalent atoms: $-x+2$, $-y$, $-z+2$.
U_{eq} is defined as one third of the trace of the orthogonalized U_{ij} tensor.

centred at δ 1.23 and δ 1.20 ppm assigned to the inequivalent *iso*-propyl methyl groups. A single crystal X-ray diffraction study on complex **3** confirmed the molecular architecture for this new complex.

A perspective view of complex **3** is shown in Fig. 2, with selected bond lengths and angles given in Table 5. As expected, the ferrocenyl group is appended to a cage carbon atom, with the ruthenium *p*-cymene fragment occupying the twelfth vertex in the MC_2B_9 icosahedron. The η-bound *p*-cym ligand is slightly tilted, lying 6° with respect to the upper C_2B_3 pentagonal belt, in response to steric demands of the upper ferrocenyl

Table 7
Selected bond lengths [Å] and angles [°] for **4**

Fe(1)–C(14)	2.045(4)	Fe(1)–C(15)	2.047(4)
Fe(1)–C(13)	2.063(4)	Fe(1)–C(11)	2.073(4)
Fe(1)–C(12)	2.073(4)	C(1)–C(11)	1.487(5)
C(1)–C(2)	1.717(5)	C(2)–C(20)	1.514(5)
C(11)–C(15)	1.419(6)	C(11)–C(12)	1.442(6)
C(12)–C(13)	1.402(7)	C(13)–C(14)	1.395(8)
C(14)–C(15)	1.426(7)	Cp1–Fe(1)	1.686
C(11)–C(1)–B(5)	124.9(3)	C(11)–C(1)–B(4)	123.2(3)
C(11)–C(1)–C(2)	115.9(3)	C(11)–C(1)–B(6)	118.0(3)
C(11)–C(1)–B(3)	115.7(3)	C(20)–C(2)–B(7)	122.4(3)
C(20)–C(2)–B(11)	121.2(3)	C(20)–C(2)–C(1)	117.9(3)
C(20)–C(2)–B(3)	118.2(3)	C(20)–C(2)–B(6)	116.8(3)
C(15)–C(11)–C(12)	107.1(4)	C(15)–C(11)–C(1)	127.8(4)
C(12)–C(11)–C(1)	124.7(4)	C(13)–C(12)–C(11)	108.0(4)
C(14)–C(13)–C(12)	108.6(4)	C(13)–C(14)–C(15)	108.7(4)
C(11)–C(15)–C(14)	107.5(4)		

Table 8
Atomic coordinates ($\times 10^4$) and equivalent isotropic displacement parameters ($Å^2 \times 10^3$) for *anti*-**6**

	x	y	z	U_{eq}
Fe(1)	10 000	0	10 000	29(1)
Ru(3)	7509(1)	197(1)	6541(1)	29(1)
C(1)	8008(11)	−577(13)	7957(9)	30(4)
C(2)	6616(11)	−166(14)	7487(10)	37(4)
B(4)	8289(16)	−1447(16)	7123(12)	36(4)
B(5)	8101(15)	−2049(15)	8156(12)	33(4)
B(6)	7062(15)	−1230(16)	8401(13)	37(4)
B(7)	5981(17)	−810(17)	6358(14)	44(5)
B(8)	7075(16)	−1637(16)	6148(14)	41(5)
B(9)	7518(16)	−2735(16)	7039(13)	40(4)
B(10)	6736(18)	−2622(20)	7788(15)	54(6)
B(11)	5861(17)	−1456(17)	7392(14)	43(5)
B(12)	6108(18)	−2350(18)	6562(14)	48(5)
C(31)	8825(11)	236(13)	8648(9)	34(3)
C(32)	9898(13)	456(13)	8629(10)	35(4)
C(33)	10363(15)	1393(14)	9309(11)	44(4)
C(34)	9551(17)	1693(16)	9670(12)	57(5)
C(35)	8609(16)	1000(15)	9315(11)	50(5)
C(21)	6154(17)	910(14)	7808(12)	52(5)
C(41)	7383(13)	2222(12)	6319(10)	33(4)
C(42)	6686(13)	1628(13)	5507(10)	37(4)
C(43)	7137(13)	738(14)	5084(12)	42(4)
C(44)	8231(13)	435(14)	5432(11)	42(4)
C(45)	8919(13)	1003(12)	6270(10)	33(3)
C(46)	8479(13)	1899(13)	6679(11)	36(4)
C(51)	6880(13)	3205(13)	6682(10)	33(3)
C(52)	6574(19)	4186(18)	5947(15)	74(6)
C(53)	7601(19)	3697(20)	7636(15)	80(6)
C(54)	8667(16)	−481(16)	4925(14)	59(5)

Symmety transformations used to generate equivalent atoms: $-x+2$, $-y$, $-z+2$.
U_{eq} is defined as one third of the trace of the orthogonalized U_{ij} tensor

cyclopentadienyl ring, which itself has twisted ($\theta = 81.7°$) away from the conformation found in compound **1** now lying essentially parallel with the cage carbon atoms. As with compound **1**, one of the hydrogen atoms on the lower cyclopentadienyl group lies close to two of the cage hydrogen atoms, H(51)–H(5) 2.752 and H(51)–H(6) 2.703 Å, although in **3** the orientation of the appended ferrocenyl group is determined by the proximity of the capping *p*-cymene ligand. The ruthenium sits 1.609Å above the upper C_2B_3 pentagonal belt, while the Ru–B distances at 2.200(7) [Ru–B(4)], 2.190(7) [Ru–B(7)] and 2.218(7) Å [Ru–B(8)] are similar to those found in 1-Ph-3-(*p*-cym)-3,1,2-*closo*-$RuC_2B_9H_{10}$ [18]. Ru(3)–C(1) is slightly longer than Ru(3)–C(2) at 2.201(6) and 2.163(6) Å, respectively. The cage C–C connectivity is 1.655(8) Å, the same as that found in 1-Ph-3-(*p*-cym-3,12-*closo*-$RuC_2B_9H_{10}$ at 1.656(6) Å. The C(1)–C(41) bond length at 1.484(8) Å is similar to that found in 7-{(η^5-C_5H_4)Co(η^5-C_5H_5)}-7,8-*nido*-$C_2B_9H_{11}$ and the precursor complex **1**. The Fe(1)–C(41) length [2.075(6) Å] is slightly longer than

Table 9
Selected bond lengths [Å] and angles [°] for *anti*-**6**

Fe(1)–C(34)	2.04(2)	Fe(1)–C(33)	2.05(2)
Fe(1)–C(32)	2.089(14)	Fe(1)–C(35)	2.09(2)
Fe(1)–C(31)	2.100(13)	Ru(3)–C(2)	2.16(2)
Ru(3)–C(43)	2.17(2)	Ru(3)–B(4)	2.18(2)
Ru(3)–C(1)	2.192(13)	Ru(3)–C(44)	2.19(2)
Ru(3)–B(8)	2.21(2)	Ru(3)–C(45)	2.21(2)
Ru(3)–B(7)	2.23(2)	Ru(3)–C(42)	2.27(2)
Ru(3)–C(46)	2.30(2)	Ru(3)–C(41)	2.350(14)
C(1)–C(31)	1.52(2)	C(1)–B(5)	1.72(2)
C(1)–B(4)	1.74(2)	C(1)–B(6)	1.76(2)
C(1)–C(2)	1.76(2)	C(2)–C(21)	1.52(2)
C(31)–C(32)	1.42(2)	C(31)–C(35)	1.43(2)
C(32)–C(33)	1.47(2)	C(33)–C(34)	1.39(3)
C(34)–C(35)	1.40(3)	C(41)–C(46)	1.39(2)
C(41)–C(42)	1.42(2)	C(41)–C(51)	1.50(2)
C(42)–C(43)	1.43(2)	C(43)–C(44)	1.38(2)
C(44)–C(45)	1.43(2)	C(44)–C(54)	1.52(2)
C(45)–C(46)	1.42(2)	C(51)–C(53)	1.53(3)
C(51)–C(52)	1.53(2)	Cp1–Fe(1)	1.671
C(2)–Ru(3)–C(43)	137.5(6)	C(2)–Ru(3)–B(4)	81.3(6)
C(2)–Ru(3)–C(1)	47.8(5)	B(4)–Ru(3)–C(1)	46.8(6)
C(2)–Ru(3)–B(8)	81.2(7)	B(4)–Ru(3)–B(8)	47.3(7)
C(1)–Ru(3)–B(8)	80.6(6)	C(2)–Ru(3)–B(7)	47.6(6)
B(4)–Ru(3)–B(7)	82.6(7)	C(1)–Ru(3)–B(7)	82.1(6)
B(8)–Ru(3)–B(7)	48.5(7)	C(31)–C(1)–B(5)	119.7(12)
C(31)–C(1)–B(4)	125.2(12)	C(31)–C(1)–B(6)	114.6(11)
C(31)–C(1)–C(2)	119.1(12)	C(31)–C(1)–Ru(3)	108.6(9)
C(21)–C(2)–C(1)	123.4(13)	C(21)–C(2)–B(6)	111.8(12)
C(21)–C(2)–Ru(3)	114.2(11)	C(32)–C(31)–C(35)	109.5(13)
C(32)–C(31)–C(1)	123.4(13)	C(35)–C(31)–C(1)	126.6(14)
C(31)–C(32)–C(33)	106.7(14)	C(34)–C(33)–C(32)	106(2)
C(33)–C(34)–C(35)	113(2)	C(34)–C(35)–C(31)	105(2)
C(46)–C(41)–C(42)	118.1(14)	C(46)–C(41)–C(51)	125.1(13)
C(42)–C(41)–C(51)	116.6(13)	C(43)–C(44)–C(45)	118(2)
C(43)–C(44)–C(54)	120(2)	C(45)–C(44)–C(54)	122.2(14)
C(46)–C(45)–C(44)	119.5(14)	C(41)–C(46)–C(45)	122.5(14)
C(41)–C(51)–C(53)	114.8(14)	C(41)–C(51)–C(52)	109.2(13)
C(53)–C(51)–C(52)	109(2)		

the other distances found between Fe(1) and the substituted cyclopentadienyl ring, a feature that has been noted previously for analogous metallocene substituted carborane systems [9]. The carbon–carbon bond lengths in the C(41)–C(45) ring are essentially the same, ranging between 1.406(10) and 1.438(10) Å, while those found in the C(51)–C(55) ring are slightly shorter 1.34(2)–1.43(3) Å and span a wider range, again presumably reflecting the greater thermal libration of these carbon atoms in the lower cyclopentadienyl ring.

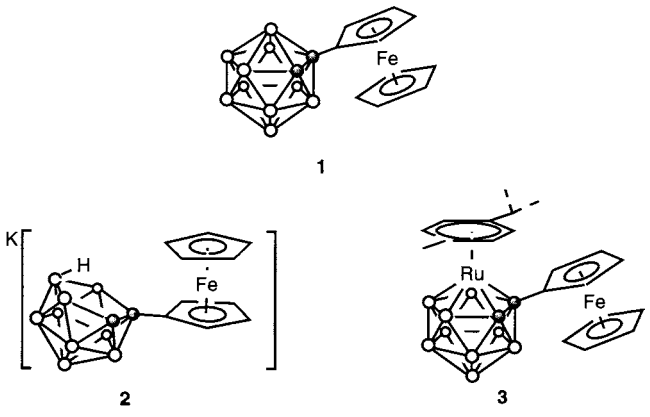

Scheme 1. Structures of compounds **1**–**3**.

3.2. Synthesis and characterisation of bis-substituted carboryl ferrocenes

In a similar procedure to that used in the synthesis of compound **1**, reaction between 1,1′-bis(methylethynyl)-ferrocene [12] and two equivalents of $B_{10}H_{14}$ in refluxing toluene in the presence of *N*,*N*-dimethylaniline affords 1,1′-{*Fc*′}-{2-Me-1,2-*closo*-$C_2B_{10}H_{10}$}$_2$ **4** in moderate yield [*Fc*′ = (η^5-C_5H_4)Fe(η^5-C_5H_4)]; a compound in which two carborane cages are linked by a ferrocenyl moiety (Scheme 2). Compound **4** was characterised by mutlinuclear NMR spectroscopy and X-ray crystallography, a perspective view is shown in Fig. 3, with salient bond lengths and angles given in Table 7.

In the solid state the molecule resides on a crystallographic inversion centre, centred around Fe(1), with a approximate, non-crystallographic, plane of mirror symmetry passing through C(20)–C(2)–C(1)–C(11) and Fe(1), giving the molecule overall approximate C_{2h} symmetry. The carborane cage adopts a conformation such the that lower ferrocenyl ring is now orientated away from C(2) ($\theta = 15.6°$), twisted essentially 180° around C(1)–C(11) compared with compound **1**, in order to minimise steric interactions between the cage bound methyl and the ferrocenyl group. The cage carbon connectivity at 1.717(5) Å is slightly longer than that found in 1-Ph-2-Me-*closo*-1,2-$C_2B_{10}H_{10}$ [19] at 1.696(5) Å and significantly longer than that found in **1**, due to the increased steric demands between the ferrocenyl and methyl groups. The C(1)–C(11) distance at 1.487(5) Å is slightly shorter than that in 1-Ph-2-Me-*closo*-1,2-$C_2B_{10}H_{10}$ [1.514(5) Å] and essentially the same as that found in **1**. The boron–boron distances lie in the range 1.759(6)–1.785(7) Å, while boron–carbon distances are in the range 1.702(6)–1.740(6) Å. The Fe–C distances range between 2.045(4) and 2.073(4) Å, being slightly longer than the equivalent bonds in compound **1**, while carbon–carbon distances in the cyclopentadienyl ring range between 1.395(8) and 1.442(6) Å. The solution NMR data is in good agreement with the solid state structure, the two methyl groups observed as a single integral six singlet in the ^{1}H-NMR spectrum. Likewise, the ^{11}B{^{1}H}-NMR spectrum displays only four signals in the ratio 1:1:4:4 between 1.80 and −6.27 ppm, further demonstrating that the two carborane cages are equivalent in solution.

Deboronation of compound **4**, using 2.5 equivalents of KOH per cage resulted in the isolation of the new

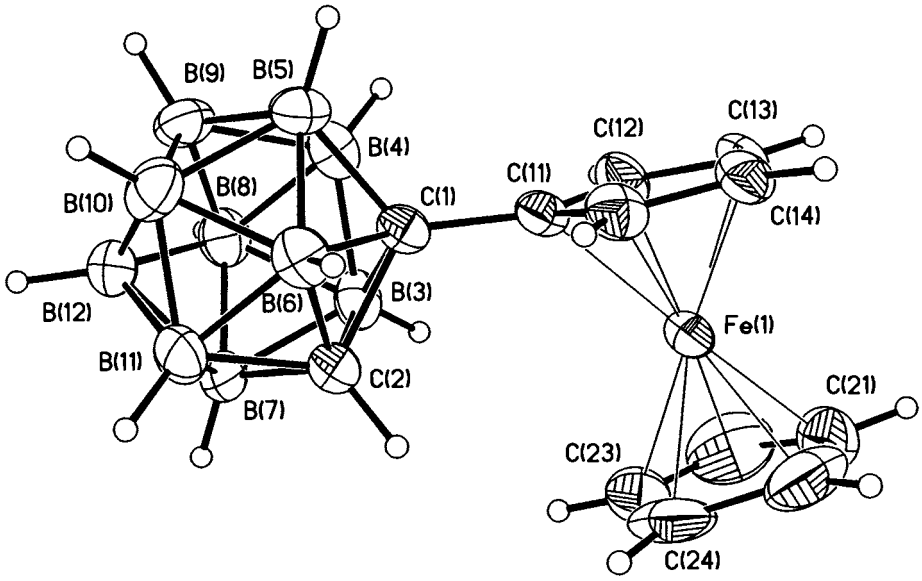

Fig. 1. Perspective view of compound **1** with atom labelling. Thermal ellipsiods are given at the 30% probability level.

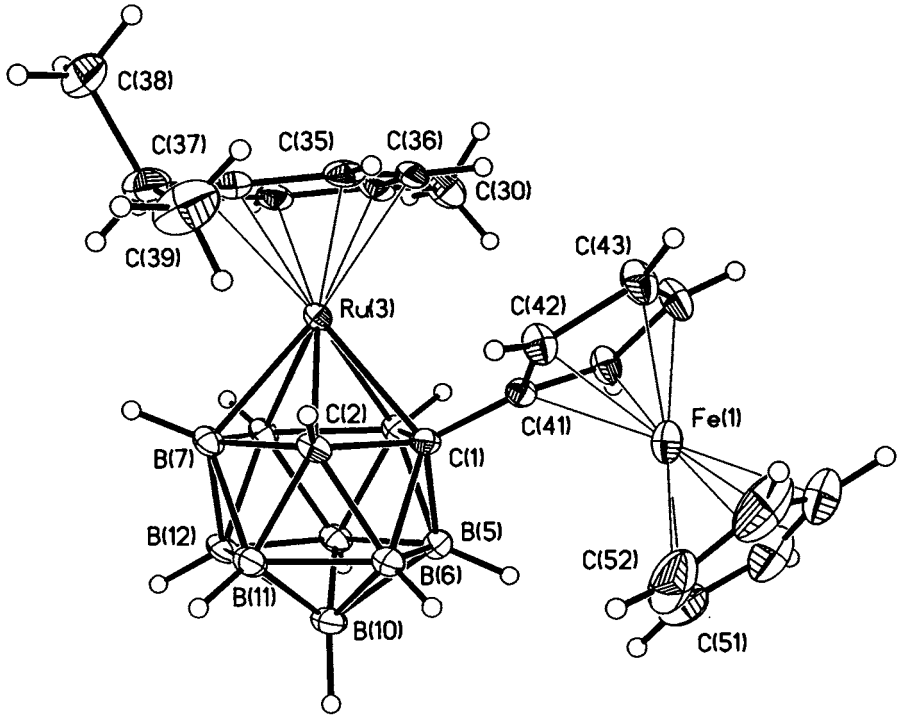

Fig. 2. Perspective view of compound **3** with atom labelling. Thermal ellipsiods are given at the 30% probability level.

complex $[7,7'\text{-}\{Fc'\}\text{-}(8\text{-Me-}7,8\text{-}nido\text{-}C_2B_9H_{10})_2]^{2-}$, **5**, isolated conveniently as the trimethylammonium salt. The $^{11}B\{^1H\}$-NMR spectrum of complex **5** demonstrates the overall *nido* structural motif, eight peaks observed in the range δ −6.61–δ −33.90 ppm, in the ratio 2:1:1:1:1:1:1:1. The ^1H-NMR spectrum shows a set of complicated multiplets, between δ 4.10 and δ 3.71 ppm, assigned to the ferrocenyl protons, while the C_{cage}-methyl protons are seen as two equal intensity singlets at 0.78 and 0.72 ppm. Double deboronation of **4**, in principle, can lead to a pair of diastereoisomers as either B(6) or B(3) can be removed. Removal of B(6) and B(3A) would lead to a product in which the methyl groups were on the same side (the *syn* isomer), whilst removal of B(6) and B(6A) would lead to methyl groups on opposite sides (*anti* isomer). In the *syn* and *anti* isomers the methyl groups are equivalent, related by a C_2 rotation or an inversion, respectively, through Fe(1). Clearly, deboronation of **4** results in the formation of each diastereoisomer in approximately equal amounts.

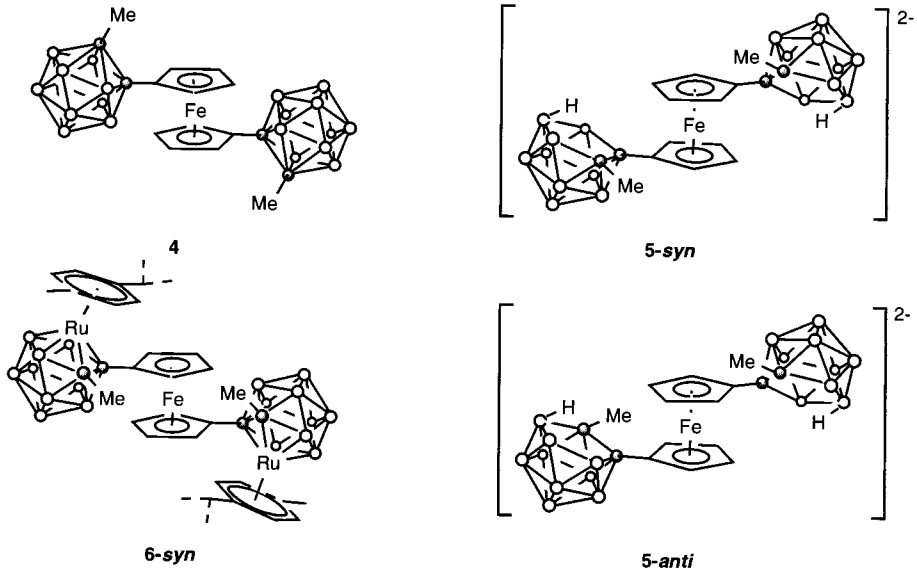

Scheme 2. Structures of compounds **4**, **5** (*syn* and *anti*) and **6**-*syn*.

Deprotonation of complex **5** (as a mixture of *syn* and *anti* isomers), and reaction with $[RuCl_2(p\text{-cym})]_2$ results in the isolation in low yield of the orange trimetallic compound 1,1′-{*Fc*′}-{2-Me-3-(*p*-cym)-3,1,2-*closo*-$RuC_2B_9H_9\}_2$, **6**, as the only mobile band under the conditions used for work-up by preparative TLC. As expected compound **6** is formed as a mixture of two diastereoisomers, inseparable by chromatography. The ^{1}H-NMR spectrum shows signals due to two very similar species in solution, in an approximate 1:1 ratio. In particular, resonances due to two sets of *p*-cymene and cage methyl protons are seen, indicating that for each diastereoisomer, both the C_{cage}-methyl groups, and *p*-cymene ligands are equivalent in solution. Fractional crystallisation at 4°C, afforded a crystalline solid which was one pure diastereoisomer by ^{1}H-NMR spectroscopy, shown by a X-ray diffraction study to be *anti*-**6** (see later). We were unable to isolate the *syn* isomer free from *anti*-**6**, chemical shifts for the *syn* isomer assigned by inspection of the ^{1}H-NMR spectra of the mixture and pure *anti*-**6**. The $^{11}B\{^1H\}$-NMR spectrum of *anti*-**6** shows five resonances in the range δ 5.42– − 10.57 ppm consistent with a *closo*-MC_2B_9 structure, while chemical shifts for the *syn* isomer could not be accurately determined due to the presence of *anti*-**6** in the sample, although the pattern of chemical shifts for both diastereoisomers is clearly very similar.

The solid state molecular structure of *anti*-**6** is shown in Fig. 4, with selected bond lengths and angles given in Table 9. Despite repeated attempts, only small, weakly diffracting crystals were available for analysis. Consequently, due to the low number of observed reflections (2739 unique data collected, 1509 observed) only the iron, ruthenium, ferrocenyl and cage carbon atoms were refined anisotropically. Never-the-less, the structural solution is unambiguous, showing the structure of this isomer to be *anti*. The molecule resides upon a crystallographically imposed centre of inversion at Fe(1). The cage carbon distance, 1.76(2) Å, is longer than that found in compound **3**, but similar to that found in 1-Ph-2-Me-3-(*p*-cym)-3,1,2-$RuC_2B_9H_9$, [18] [1.754(11) Å]. The ruthenium atom sits 1.596 Å above the C_2B_3 face, while the *p*-cym fragment is tilted by 11.2°, significantly more than found in **3**, due to steric pressure from the cage bound methyl group. The ferrocenyl group is twisted from lying parallel with the cage carbon atoms ($\theta = 58.4°$) in response to this steric pressure. Similar to the situation found in **3**, the ferrocenyl group is orientated so that one of the cage hydrogen atoms [H(5)] fits between two of the ferrocenyl protons [H(34A) and H(33A)].

3.3. Electrochemistry

The closo compounds **1**, **3**, **4** and **6** were studied electrochemically, in a preliminary investigation. Additionally the parent fragment 3-(*p*-cym)-3,1,2-*closo*-$RuC_2B_9H_{11}$ [18] was also studied for comparison with the new compounds reported here. In CH_2Cl_2 (− 1.80– + 1.80 V), 3-(*p*-cym)-3,1,2-*closo*-$RuC_2B_9H_{11}$ was found to show no significant electrochemical activity [unlike the analogous compound (*p*-cym)Ru(η^5-$Et_2C_2B_4H_4$)] [20], thus limiting the discussion of results for the new compounds to the ferrocenyl moiety only. The new compounds studied all displayed the expected reversible oxidation wave attributable to the Fe^{II}–Fe^{III} oxidation process. The addition of one carborane cage to ferrocene (compound **1**) resulted in a positive shift for the Fe^{II}–Fe^{III} couple, $E_{1/2} + 0.243$ V (with reference to internal ferrocene/ferrocenium), while the addition of

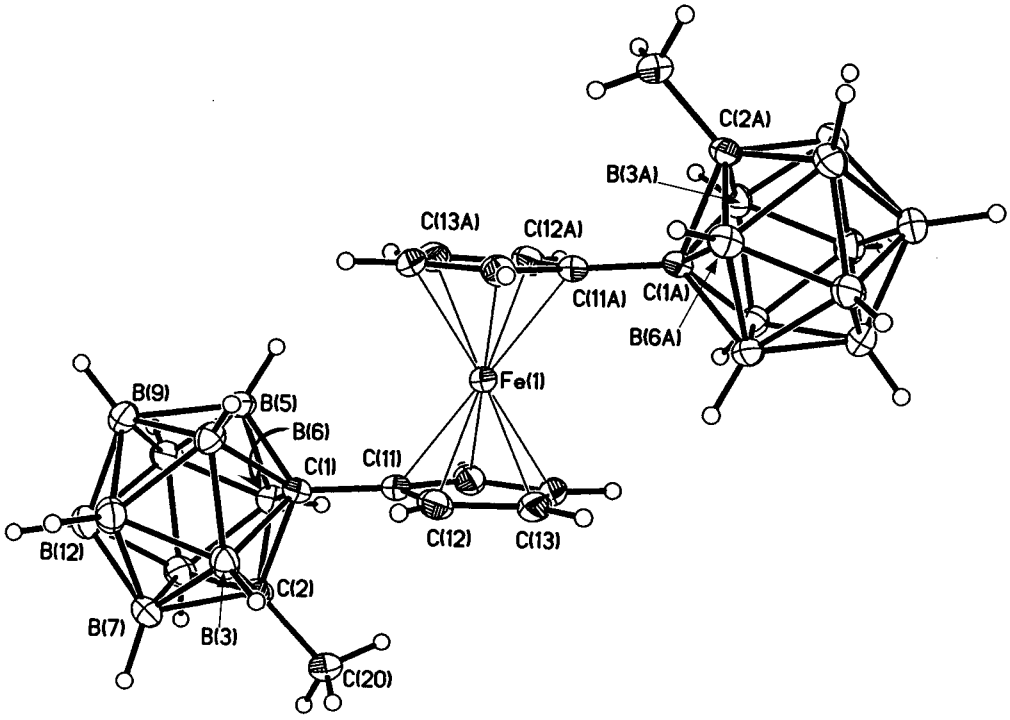

Fig. 3. Perspective view of compound **4** with atom labelling. Thermal ellipsiods are given at the 30% probability level. Atoms suffixed 'A' are generated by crystallographically imposed inversion.

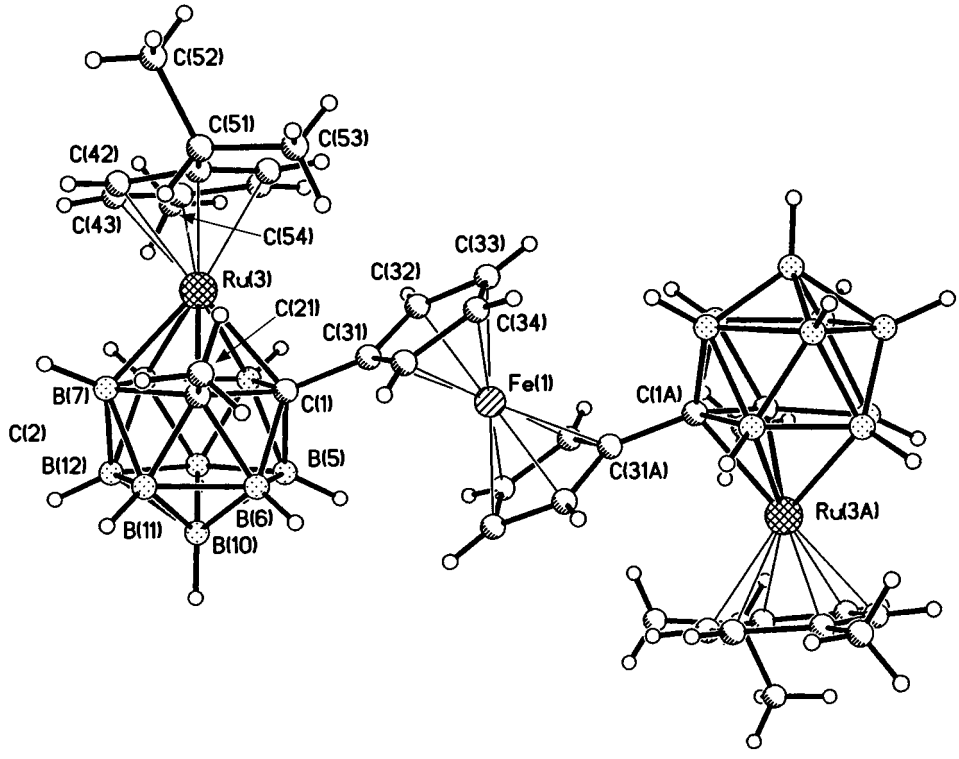

Fig. 4. Perspective view of compound **6** with atom labelling. Atoms suffixed 'A' are generated by crystallographically imposed inversion.

another cage caused the magnitude of this shift to effectively double, $E_{1/2}$ for compound **3** measured as $+0.551$ V. These results are fully consistent with carborane cages being regarded as formally electron deficient. Replacement of one {BH} vertex (in compound **3**) or two {BH} vertices (in **6**) with {Ru(*p*-cym)} gives $E_{1/2}$ values of $+0.036$ and $+0.068$ V, respectively. This is a negative shift of 198 and 483 mV compared with the

precursor complexes **1** and **4**, respectively, reflecting the fact that the {Ru(*p*-cym)} is relatively electron rich compared with {BH} and consequentally the cage moiety now exerts less of a negative inductive effect compared with *closo*-C_2B_{10}.

4. Conclusion

We have demonstrated that mono- and bis-ethynyl ferrocences may be reacted with decaborane to afford mono- or bis-carborane substituted ferrocenes, respectively. Deboronation and metallation of these new species results in the isolation of novel bi- and tri-metallic ferrocenylmetallacarboranes. These new complexes represent a starting point for the further investigation of (metalla)carboranes which have the added functionality of a σ-bound pendant metallocene or cyclopentadienyl group. Further contributions intended to develop this theme further.

Acknowledgements

We thank ERASMUS (CLB) for an exchange scholarship from the Philipps University, Marburg, Germany; Heriot-Watt University, the EPSRC (ASW and GMR, respectively) for financial support and the Callery Chemical Company for its continued support of heteroborane research at Heriot-Watt. Drs Alan Brown and Stuart McGregor are thanked for thier help with the electrochemical experiments. Two of us (CLB and ASW) would also like to thank Professor Alan Welch for valuable support and the generous provision of laboratory facilities.

References

[1] (a) M.J. Begley, P. Mountford, P.J. Stewart, D. Swallow, S. Wan, J. Chem. Soc. Dalton Trans. (1996) 1323. (b) R.J. Less, J.L.M. Wicks, N.P. Chatterton, M.J. Dewey, N.L. Cromhout, M.A. Halcrow, J.E. Davies, J. Chem. Soc. Dalton Trans. (1996) 4055.
[2] (a) N. J. Long, Angew. Chem. Int. Ed. Engl. 34 (1995) 21; M.D. Ward, Chem. Soc. Rev. 24 (1995) 121. (b) A. Togni, T. Heayashi (Eds.), Ferrocenes, VCH, Weinham, Germany, 1995.
[3] (a) P.A. Chetcuti, W. Hofherr, A. Liegard, G. Rihs, G. Rist, H. Keller, D. Zech, Organometallics 14 (1995) 666. (b) Y.K. Yan, D.M.P. Mingos, W.S. Li, I.J. Scowen, M. McPartlin, A.T. Coomber, R.H. Friend, J. Chem. Soc. Dalton Trans. (1995) 2851. (c) Rh. Ll. Thomas, G.M.R. Rosair, A.J. Welch, J. Chem. Soc. Chem. Commun. (1996) 1327. (d) K.J. Donaghy, P.J. Carroll, L.G. Sneddon, Inorg. Chem. 36 (1997) 547.
[4] (a) W. Jiang, C.B. Knobler, M.F. Hawthorne, Angew. Chem Int. Ed. Engl. 35 (1996) 2536. (b) X. Yang, S.E. Johnson, S.I. Khan, M.F. Hawthorne, ibid 31 (1992) 893.
[5] (a) J. Plesek, Chem. Rev. 92 (1992) 269. (b) R.N. Grimes, Chem. Rev. 92 (1992) 251.
[6] R.N. Grimes, Appl. Organomet. Chem. 10 (1996) 209.
[7] L.I. Zakharkin, V.N. Kalinin, A.P. Snyakin, Zh. Obshch. Khim. 40 (1970) 2246.
[8] M.R. Churchill, B.G. BeBoer, J. Am. Chem. Soc 96 (1974) 6310.
[9] R.N. Grimes, W.M. Maxwell, R.B. Maynard, E. Sinn, Inorg. Chem. 19 (1980) 2981.
[10] L.I. Zakharkin, L.V. Orlova, B.V. Lokshin, L.A. Fedrov, J. Organomet. Chem. 40 (1972) 15.
[11] I.T. Chizhevsky, A.I. Yanovshy, Y.T. Struchkov, J. Organomet. Chem. 536 (1997) 51.
[12] G. Doisneau, G. Balavoine, T. Fillebeen-Khan, J. Organomet. Chem. 425 (1992) 113.
[13] Adapted from: M.A. Bennett, T.-N, Huang, H.M. Doesbury, T.W. Matheson, A.K. Smith, Inorg. Synth. 21 (1982) 74.
[14] SHELXTL, PC version 5.0, Siemens Analytical Instruments, Madison, WI, 1994.
[15] (a) P.T. Brain, J. Cowie, D.J. Donohoe, D. Hynk, D.W.H. Rankin, D. Reed, B. D. Reid, H.E. Robertson, M. Hofmann, P. von-Ragué Schleyer, A.J. Welch, Inorg. Chem. 35 (1996) 1710. (b) G.M. Rosair, Rh. Ll. Thomas, A.J. Welch, Acta Crystallogr. C52 (1996) 1024.
[16] Z.G. Lewis, A.J. Welch, Acta Crystallogr. C49 (1993) 705.
[17] M.F. Hawthorne, D.C. Young, P.M. Garrett, D.A. Owen, S.G. Schwerin, F.N. Tebbe, P.A. Wegner, J. Am. Chem. Soc. 90 (1968) 862.
[18] J. Cowie, B.D. Reid, J.M.S. Watmough, A.J. Welch, J. Organomet. Chem. 481 (1994) 283.
[19] T.D. McGrath, A.J. Welch, Acta Crystallogr. C51 (1995) 646.
[20] J.W. Merket, W.E. Geiger, M.D. Atwood, R.N. Grimes, Organometallics 10 (1991) 3545.